2009 IEEE International Conference on Robotics and Automation
Kobe International Conference Center
Kobe, Japan, May 12-17, 2009

Torque Modeling and Analysis of Spherical Actuators with Iron Stator

Liang Yan, *Member, IEEE*, I-Ming Chen, *Senior Member, IEEE*, Chee Kian Lim,
Guilin Yang, *Member, IEEE* Wei Lin, *Member, IEEE* and Kok-Meng Lee, *Fellow, IEEE/ASME*

***Abstract*— This paper presents a ball-joint-like three-degree-of-freedom (3-DOF) permanent magnet (PM) spherical actuator which features a ball-shaped rotor with multiple PM poles and a spherical iron stator with air-core coils. Torque output of this PM spherical actuator is formulated analytically. Based on the torque model, simulation result of the actuator torque variation is presented. In addition, the effect of the stator iron on the torque output is evaluated.**

I. Introduction

Compared with conventional three-degree-of-freedom (3-DOF) spherical motion mechanism by using several single-axis actuators connected in parallel or in series, a spherical actuator that can generate multi-DOF rotational motion in one joint has the advantages of compact structure, fast response and singularity free in workspace. Unlike single-axis actuators, torque output of the spherical actuator has three components. Because all torque components are dependant on rotor orientation, obtaining actuator torque in terms of input current to the motor coils becomes a complicated problem. Williams and Laithwaite [1] [2] have designed the first 2-DOF spherical induction motor. Magnetic field generated by stator windings induces a current on the rotor surface, and causes the rotor to incline. Davey *et al.* [3] derived the torque model of this induction motor by integrating the Maxwell stress moment over the spherical rotor surface and proposed its use as a robot wrist [4]. The mechanical complexity and the inherent poor servo characteristics of the spherical induction motor led Lee *et al.* [5] to develop a 3-DOF spherical stepper based on the principle of variable-reluctance. The torque output of a variable-reluctance spherical motor (VRSM) depends on the current inputs as well as the magnetic reluctance at the air-gaps between the rotor and the stator poles [6]. The torque model of this motor is obtained by differentiating coenergy with respect to the angular displacement parameters. In the past decade, several variations of spherical motors with a structure similar to [5] have been studied. Wang *et al.* [7]–[10] have developed spherical actuators achieving 2/3-DOF motions. The rotor is a completely magnetized ball. Coils are uniformly mounted on the stator. The torque models of these spherical actuators were obtained by using Lorentz force law. Chirikjian *et al.* [11] have made a spherical stepper with a permanent magnet (PM) pole rotor and a stator with an array of coils. Difference in the symmetric layout of the rotor poles and the stator poles allows stepping motion in three orientations. Kahlen *et al.* [12] developed a spherical motor consisting of a rotor sphere with 112 PM poles and an outer stator with 96 stator windings. The torque produced by the stator winding was calculated numerically. More recently, Lee *et al.* [13] [14] have developed a spherical wheel motor that offers a means to control the orientation of its shaft in an open-loop fashion.

In our previous study [15] [16], a research prototype of PM spherical actuator has been developed as shown in Fig. 1.

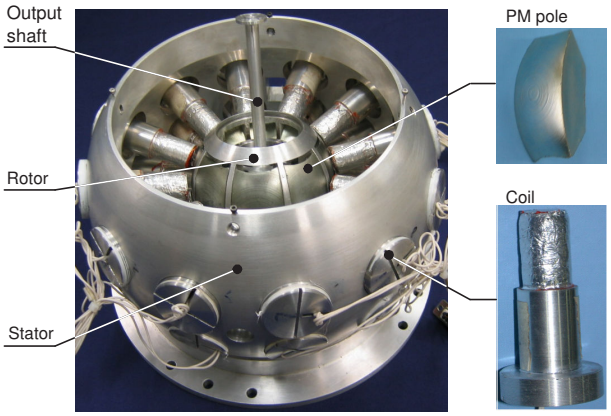

Fig. 1. Prototype of spherical actuator

TABLE I
Structure specifications of spherical actuator

Inner / outer stator radius	95 / 112.5 (mm)
Rotor radius	46.5 (mm)
Rotor core radius	23 (mm)
PM pole parameters	α=40°, β = 70°
Number of rotor poles (PM)	8
Number of stator poles (coil)	24 / 2 layers
Number of coil turns	1027
Maximum tilting angle	±11°
Maximal spinning torque	4 (Nm)
Maximal tilting torque	0.8 (Nm)

This work was supported by a collaborative research project under Grant U02-A-O40B for Nanyang Technological University, Singapore Institute of Manufacturing Technology, and Georgia Institute of Technology.

L. Yan, I-M. Chen and C.-K. Lim are with the School of Mechanical and Aerospace Engineering, Nanyang Technological University, Singapore 637098 (e-mail: yanliang@pmail.ntu.edu.sg; michen@ntu.edu.sg; cklim@ntu.edu.sg).

G. Yang, W. Lin are with Mechatronics Group, Singapore Institute of Manufacturing Technology, 71 Nanyang Drive, Singapore 638075 (e-mail: glyang@simtech.a-star.edu.sg; wlin@simtech.a-star.edu.sg).

K.-M. Lee is with George W. Woodruff School of Mechanical Engineering, Georgia Institute of Technology, Atlanta, Georgia, USA 30332-0405. (e-mail: kokmeng.lee@me.gatech.edu).

The specification is listed in Table I. The key feature of this spherical actuator is its flexible structure, i.e., the relationship between the torque output and structure parameters can be described so that optimum values of parameters can be selected to achieve high torque output [17]. Furthermore, more PM and coil poles may be incorporated, thereby increasing the working range (up to $45°$) and motion resolution of the actuator. In this prototype, the stator is made from aluminum for preliminary study. As ferromagnetic materials such as soft iron may reduce the magnetic energy loss and increase the actuator torque, the objective of this paper is to derive the torque output of PM spherical actuators with a laminated-soft-iron stator by using Laplace's equation and Lorentz force law. Furthermore, the effect of stator iron on the actuator torque output is analyzed. The modeling method can be used for other similar designs.

II. Working Principle

The working principle of the spherical actuator is illustrated in Fig. 2. The rare earth PMs (NdFeB) mounted along the rotor equator can produce high flux density. The air-core coils are assembled on the stator which can simplify the torque model of the spherical actuator in a linear fashion. By activating pairs of coils in two longitudinal directions, the rotor can tilt in two orthogonal directions as shown in Fig. 2(a) and 2(b). Energizing all circumferential coils, the rotor can spin about its own axis (Fig. 2(c)). Therefore, by varying the input currents of coils, any desirable 3-DOF spherical motion within the workspace can be achieved.

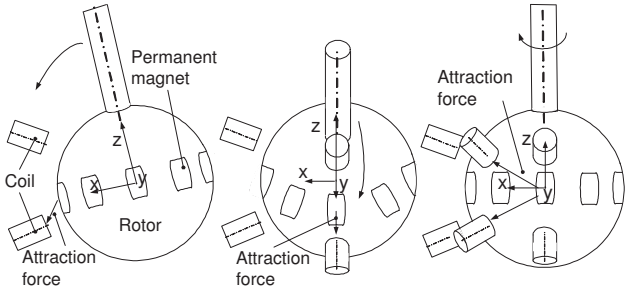

(a) First tilting motion (b) Second tilting motion (c) Spinning motion

Fig. 2. 3-DOF motion of spherical actuator

III. Formulation of Magnetic Field

A. Assumptions

Assumptions that are useful for the formulation of magnetic field are listed as follows.

- The magnetic permeability of air space is the same as that of free space.
- The magnetic permeability of stator iron is much greater than that of air space.
- PMs are assumed to be ideal with field relationship described by the linear second quadrant of a PM demagnetization curve.

B. Characterization of Rotor Space

In formulating the magnetic field of the rotor, we use a generic spherical rotor model as shown in Figure 3 for discussion. The PM poles are evenly spaced (with alternate polarities) around the rotor equator, each of which has the shape of a dihedral cone defined in terms of four parameters: longitudinal angle α, latitudinal angle β, outer and inner radii, R_r and R_b. With such an arrangement, the study of rotor magnetic field can be divided into three parts.

1) Air Space outside the Rotor (Region 1): The air gap is a linear homogeneous media with the absence of magnetization, which can be characterized by a constitutive relation

$$\mathbf{B}_1 \quad = \quad \mu_0 \mathbf{H}_1, \tag{1}$$

where the subscript "1" denotes Region 1; $\mathbf{B}$ and $\mathbf{H}$ are the magnetic flux density and field intensity; and μ_0 is permeability of free space with a value of $4\pi \times 10^{-7}$H/m.

2) Within the Dihedral PM Rotor Poles (Region 2): In this study, PMs are assumed to be ideal with field relationship described by the linear second quadrant of a PM demagnetization curve. Therefore, the magnetic property of PM can be characterized by

$$\mathbf{B}_2 \quad = \quad \mu_0 \mu_m \mathbf{H}_2 + \mu_0 \mathbf{M}_0, \tag{2}$$

where μ_m is the dimensionless relative recoil permeability of PM (typical value ranging between 1.05 and 1.20); $\mathbf{M}_0 = \mathbf{B}_{rem}/\mu_0$ is the residual magnetization vector in A/m; and $\mathbf{B}_{rem}$ is defined as the remanence in Tesla. In spherical coordinates, the residual magnetization vector of the p^{th} PM can be expressed as

$$\mathbf{M}_0 = \begin{bmatrix} M_{0,r} \\ M_{0,\theta} \\ M_{0,\phi} \end{bmatrix} = (-1)^{p-1} |\mathbf{M}_0| \begin{bmatrix} \cos(\phi - \alpha_p)\sin\theta \\ \cos(\phi - \alpha_p)\cos\theta \\ -\sin(\phi - \alpha_p) \end{bmatrix}, \tag{3}$$

where $\alpha_p = \alpha/2 + 2\pi(p-1)/P$, $p = 1, 2, ..., P$. P is the total number of PM poles. In this study, let $P = 8$. Note that these equations are only valid within the range of

$$0 < \phi - \frac{2\pi(p-1)}{P} < \alpha, \ \frac{\pi}{2} - \frac{\beta}{2} < \theta < \frac{\pi}{2} + \frac{\beta}{2}.$$

For the non-magnetized space in between poles on the rotor, the residual magnetization is equal to zero.

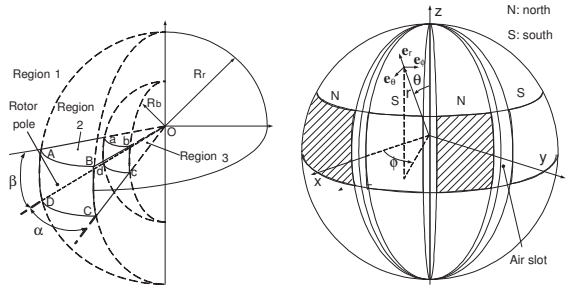

(a) Single rotor pole (b) Alternately arranged

Fig. 3. Arrangement of rotor poles

3) Rotor Core Made of Ferromagnetic Material (Region 3): The magnetic property of ferromagnetic material such as soft iron can be characterized as

$$\mathbf{B}_3 = \mu_0\mu_r\mathbf{H}_3, \tag{4}$$

where μ_r is relative permeability of the ferromagnetic core.

C. Governing Equations

For an irrotational magnetic field,

$$\nabla \times \mathbf{H} = 0, \qquad \nabla \cdot \mathbf{B} = 0, \tag{5}$$

where $\mathbf{H}$ is curl free and can be expressed in terms of a scalar potential function Φ based on Helmholtz's theorem:

$$\mathbf{H} = -\nabla\Phi. \tag{6}$$

In spherical coordinates,

$$\begin{aligned}\mathbf{H} &= H_r\mathbf{e}_r + H_\theta\mathbf{e}_\theta + H_\phi\mathbf{e}_\phi \\ &= \left[-\frac{\partial\Phi}{\partial r}, \; -\frac{1}{r}\frac{\partial\Phi}{\partial\theta}, \; -\frac{1}{r\sin\theta}\frac{\partial\Phi}{\partial\phi}\right]^T, \end{aligned} \tag{7}$$

where $\mathbf{e}_r$, $\mathbf{e}_\theta$ and $\mathbf{e}_\phi$ are respective unit vectors, H_r, H_θ and H_ϕ are components of magnetic intensity. For Regions 1 and 3, the scalar potentials are governed by Laplace's equations:

$$\nabla^2\Phi_1 = 0, \qquad \nabla^2\Phi_3 = 0. \tag{8}$$

The scalar potential Φ_2 within Region 2 is expressed as

$$\nabla^2\Phi_2 = \nabla \cdot \mathbf{M}_0/\mu_m, \tag{9}$$

which is in the form of Poisson's equation. With a symmetric arrangement of rotor poles, the divergence of the residual magnetization vector is equal to zero, i.e. $\nabla \cdot \mathbf{M}_0 = 0$. Thus, the Poisson's equation can be reduced to Laplace's equation, $\nabla^2\Phi_2 = 0$.

D. Solution of Magnetic Flux Density

By using the governing equations and the characterization of three regions, the magnetic field distribution surrounding the PM rotor can be derived as follows.

$$B_{1,r} = \frac{3}{8}\sqrt{\frac{35}{2\pi}}\frac{ac\mu_0 M_0}{\sqrt{\pi}}[5O_{4,6}r^{-6} - 4O_{4,5}r^3]\sin^4\theta\cos 4\phi, \tag{10}$$

$$B_{1,\theta} = -\frac{3}{2}\sqrt{\frac{35}{2\pi}}\frac{ac\mu_0 M_0}{\sqrt{\pi}}[O_{4,5}r^3 + O_{4,6}r^{-6}]\sin^3\theta\cos\theta\cos 4\phi, \tag{11}$$

$$B_{1,\phi} = \frac{3}{2}\sqrt{\frac{35}{2\pi}}\frac{ac\mu_0 M_0}{\sqrt{\pi}}[O_{4,5}r^3 + O_{4,6}r^{-6}]\sin^3\theta\sin 4\phi, \tag{12}$$

where M_0 is the magnitude of the residual magnetization vector $\mathbf{M}_0$. The three flux components $B_{1,r}$, $B_{1,\theta}$ and $B_{1,\phi}$ are defined in spherical coordinates as shown in Fig. 3, and

$$\begin{aligned}
O_{4,6} &= -(O_{4,3}/O_{4,4}R_r^9 - O_{4,2}/O_{4,1})/(R_r^9 - R_s^9)R_s^9, \\
O_{4,5} &= (O_{4,3}/O_{4,4}R_r^9 - O_{4,2}/O_{4,1})/(R_r^9 - R_s^9), \\
O_{4,4} &= [4(\mu_r - \mu_m)R_b^9], \\
O_{4,3} &= [4\mu_r + 5\mu_m]O_{4,2}/O_{4,1} - R_b^6 \\
O_{4,2} &= 4R_r^6(R_r^9 - R_s^9)(\mu_r - \mu_m)R_b^9 - R_b^6R_r^9\{4R_r^9(1-\mu_m) + \\
&\quad (5 + 4\mu_m)R_s^9\}, \\
O_{4,1} &= 4\{[4+5\mu_m]R_r^9 + [5-5\mu_m]R_s^9\}(\mu_r - \mu_m)R_b^9 - R_r^9 \\
&\quad \{4R_r^9(1-\mu_m) + (5+4\mu_m)R_s^9\}[4\mu_r + 5\mu_m].
\end{aligned}$$

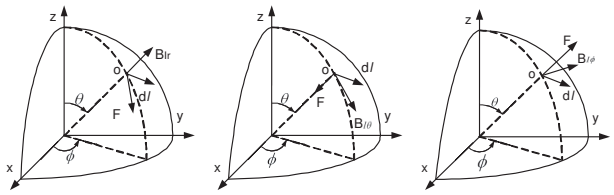

Fig. 4. Force activated by three components of the flux density

a and c in Eqns. (10)-(12) can be calculated with following equations

$$a \pm bi \equiv \int_0^{2\pi} f(\phi)e^{-im\phi}d\phi \quad (m = 4 \text{ and } m = -4), \tag{13}$$

$$c/\sqrt{\pi} \equiv \int_0^{\pi} S_n^m \sin^2\theta[P_n^m(\cos\theta)]d\theta, \tag{14}$$

where

$$\begin{aligned} f(\phi) &= (-1)^{p-1}\cos[\phi - \frac{\pi}{4}(p-1)], \; p = 1, 2, ..., 8. \\ S_n^m &= \sqrt{\frac{2n+1}{4\pi}\frac{(n-m)!}{(n+m)!}}. \end{aligned}$$

E. Magnetic Flux Component for Torque Generation

The direction of the force generated by each component of the flux density, $B_{1,r}$, $B_{1,\theta}$ and $B_{1,\phi}$ can be determined as shown in Fig. 4. The differential length segment $d\mathbf{l}$ of the wire is tangential to the spherical surface at point O. Note that only $B_{1,r}$ can produce a torque to change the rotor orientation. $B_{1,\theta}$ and $B_{1,\phi}$ do not produce torque on the rotor because the action lines of magnetic forces generated by $B_{1,\phi}$ and $B_{1,\theta}$ pass through the rotor center.

IV. Formulation of Torque Model

A. Coil Geometry

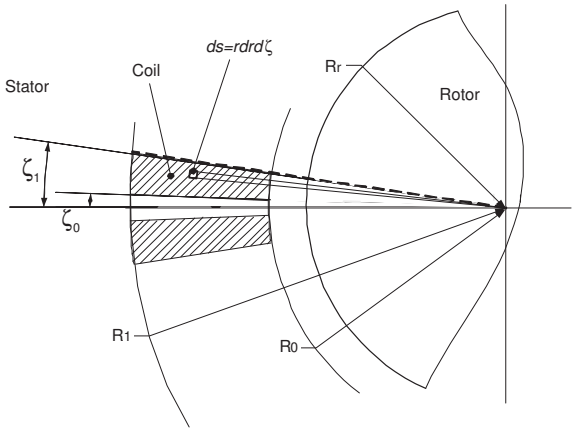

Fig. 5. Section view of the conical air-core coil

An ideal air-core coil used in the spherical actuator is illustrated in Fig. 5. The coil assumes a conical-shaped object

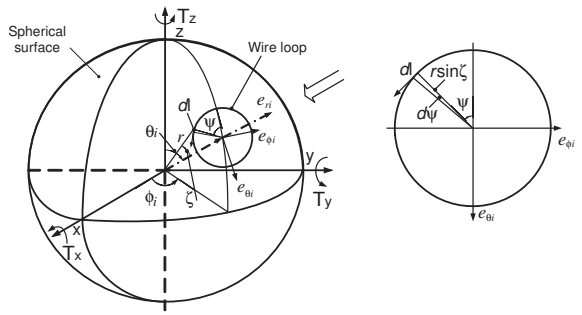

Fig. 6. One loop of wire in the i^{th} coil on the sphere

embedded in the stator shell to facilitate the formulation of the actuator torque. Without loss of generality, the dimensions of the coil (shaded region) can be specified by four quantities: R_0-center distance of the inner surface of the coil; R_1-center distance of the outer surface of the coil; ζ_0-angular diameter of the air-core and ζ_1-angular diameter of the coil.

B. Torque on Differential Line Segment of Winding

Consider a differential line segment $d\mathbf{l}$ of the winding. As shown in Fig. 5, the differential sectional area of $d\mathbf{l}$ can be computed by

$$ds = rdrd\zeta. \tag{15}$$

The current passing through this section area is $Jrdrd\zeta$, where J is the current density in the section area of the coil. According to Lorentz force law, the differential force on the rotor caused by the interaction between magnetic field of the PM-pole rotor and current carrying conductor $d\mathbf{l}$ is

$$d\mathbf{F} = -Jrdrd\zeta d\mathbf{l} \times B_{Ir}(r,\theta,\phi)\mathbf{e}_r, \tag{16}$$

where $\mathbf{e}_r$ is the unit vector in the r-direction of spherical coordinates. The negative sign indicates that the force imposed on the rotor by $d\mathbf{l}$ is the reaction force exerted by the magnetic field on $d\mathbf{l}$. It can be seen that the differential torque generated by $d\mathbf{l}$ is the cross product of the moment arm $r\mathbf{e}_r$ (the vector from rotor center to the differential winding segment) and force $d\mathbf{F}$, i.e.,

$$d\mathbf{T}_i = r\mathbf{e}_r \times [-Jrdrd\zeta d\mathbf{l} \times B_{Ir}(r,\theta,\phi)\mathbf{e}_r]. \tag{17}$$

C. Integration on Entire Coil Volume

Integrating the differential torque in Eqn. (17) within the entire volume of the coil gives the torque of a single coil under the magnetic field of PM rotor as

$$\mathbf{T}_c = -J\int_{R_0}^{R_1}\int_{\zeta_0}^{\zeta_1}\left\{\int_C rB_{Ir}(r,\theta,\phi)d\mathbf{l}\right\}rdrd\zeta. \tag{18}$$

The symbol $\int_C$ denotes the line integral of the differential torque along a circular loop of the winding that has a "wire" section area of ds.

D. Solution to Torque Integral

With analytical expression of $B_{1,r}$ and Eqn. (18), the actuator torque generated by the i^{th} coil, denoted as $\mathbf{T}_i$, can be expressed explicitly using the i^{th} coil-axis position θ_i and ϕ_i with respect to the rotor frame, as well as the current input J_i passing through this coil. For any rotor orientation, the torque output can then be determined by the current input uniquely. Assume that only one coil is mounted on the stator. The spherical coordinates (θ_i, ϕ_i) is used to represent the position of the coil in the rotor frame. One loop of winding in the i^{th} coil on the sphere is indicated in Fig. 6. The differential length segment $d\mathbf{l}$ can be calculated as

$$d\mathbf{l} = r\sin\zeta d\psi(\sin\psi\mathbf{e}_{\theta i} - \cos\psi\mathbf{e}_{\phi i}). \tag{19}$$

By substituting magnetic field component $B_{1,r}$ of Eqn. (10) and $d\mathbf{l}$ of Eqn. (19) into torque integral formula of Eqn. (18), the torque output of a single coil can be obtained as

$$\mathbf{T}_i = T_c\mathbf{G}(\theta_i,\phi_i)J_i \tag{20}$$

where

$$\begin{aligned}
\mathbf{T}_i &= [T_{ix},\ T_{iy},\ T_{iz}]^{\mathrm{T}},\\
\mathbf{G}(\theta_i,\phi_i) &= [g_x(\theta_i,\phi_i),\ g_y(\theta_i,\phi_i),\ g_z(\theta_i,\phi_i)]^{\mathrm{T}}\\
&= \mathbf{e}_{\phi i}(-4\sin^3\theta_i\cos^4\phi_i\cos\theta_i - 4\sin^3\theta_i\sin^4\phi_i\cos\theta_i\\
&\quad +24\sin^3\theta_i\cos^2\phi_i\sin^2\phi_i\cos\theta_i) - \mathbf{e}_{\theta i}(16\sin^3\theta_i\\
&\quad \cos^3\phi_i\sin\phi_i - 16\sin^3\theta_i\sin^3\phi_i\cos\phi_i),\\
T_c &= \frac{15}{8}\sqrt{\frac{35}{2}}\mu_0 M_0 acR_c G_\zeta,\\
R_c &= O_{4,6}R_{c,1} + O_{4,5}R_{c,2},\\
R_{c,1} &= (R_0^{-2} - R_1^{-2})/2,\\
R_{c,2} &= (R_0^7 - R_1^7)/7,\\
G_\zeta &= G_\zeta^{''} - \frac{3G_\zeta^{'}}{4},\\
G_\zeta^{'} &= 1/5\sin^5\zeta_1 - 1/5\sin^5\zeta_0,\\
G_\zeta^{''} &= 1/5\cos^4\zeta_0\sin\zeta_0 - 1/15\cos^2\zeta_0\sin\zeta_0 - 2/15\sin\zeta_0\\
&\quad -1/5\cos^4\zeta_1\sin\zeta_1 + 1/15\cos^2\zeta_1\sin\zeta_1 + 2/15\sin\zeta_1.
\end{aligned}$$

The unit vectors $\mathbf{e}_{\phi i}$ and $\mathbf{e}_{\theta i}$ in spherical coordinates can be represented in terms of Cartesian coordinates as

$$\begin{aligned}
\mathbf{e}_{\phi i} &= -\sin\phi_i\mathbf{e}_x + \cos\phi_i\mathbf{e}_y = \begin{bmatrix} -\sin\phi_i \\ \cos\phi_i \\ 0 \end{bmatrix},\\
\mathbf{e}_{\theta i} &= \cos\theta_i\cos\phi_i\mathbf{e}_x + \cos\theta_i\sin\phi_i\mathbf{e}_y - \sin\theta_i\mathbf{e}_z\\
&= \begin{bmatrix} \cos\theta_i\cos\phi_i \\ \cos\theta_i\sin\phi_i \\ -\sin\theta_i \end{bmatrix}.
\end{aligned}$$

E. Torque Model of Full Set of Coils

Eqn. (20) represents the torque of a single coil. With N coils on the stator, the torque model of the spherical actuator with a complete set of coils can be obtained

$$\mathbf{T} = T_c Q\mathbf{J}, \tag{21}$$

where $\mathbf{J} = \begin{bmatrix} J_1 & J_2 & \cdots & J_N \end{bmatrix}^T$ represents currents passing through N coils, and Q is defined to be the torque matrix

$$Q = \begin{bmatrix} f_x(\theta_1,\phi_1)\, f_x(\theta_2,\phi_2) \cdots f_x(\theta_N,\phi_N) \\ f_y(\theta_1,\phi_1)\, f_y(\theta_2,\phi_2) \cdots f_y(\theta_N,\phi_N) \\ f_z(\theta_1,\phi_1)\, f_z(\theta_2,\phi_2) \cdots f_z(\theta_N,\phi_N) \end{bmatrix}.$$

V. Simulation and Analysis

A. Simulation Result

The three torque components produced by a single coil can be calculated from Eqn. (20). Let $\mathbf{B}_{rem} = 1$T, $R_b = 15$mm, $R_r = 45$mm, $R_s = 80$mm, $R_s = 80$mm, $\xi_0 = 2°$, $\xi_1 = 15°$, $R_0 = 45.1$mm, $R_1 = 60$mm and J_i =3A. The variation of torque components T_x, T_y and T_z with respect to θ and ϕ are presented in Fig. 7, where θ and ϕ are used to specify the position of coil's axis in the rotor frame. Because the tilting motion of the rotor is constrained by the output shaft as well as the spherical bearing which secures the rotor position inside the stator, θ is defined in the range of $[60°, 120°]$.

From Fig. 7(b), it can be seen that when coil axis is at the rotor equator ($\theta = 90°$), only T_z will be produced, whereas T_x and T_y are equal to zero. This is coincident with the simulation result in Fig. 7(a), 7(c) and 7(e). When the coil axis shifts an angle away from the rotor equator as indicated in Fig. 7(d) and 7(f), T_x and T_y are not equal to zero. Furthermore, they have opposite directions when the coil axis is at upper and lower hemispheres. There are eight positive/negative ridges for the variation of T_z in ϕ direction, which are caused by the eight alternatively magnetized PM poles along the rotor equator. However, the variation of T_x and T_y is not in phase with the poles arrangement, because rotor coordinates are employed for the torque computation. It can be verified that if stator coordinates are used for the computation, eight ridges will appear for all three torque components.

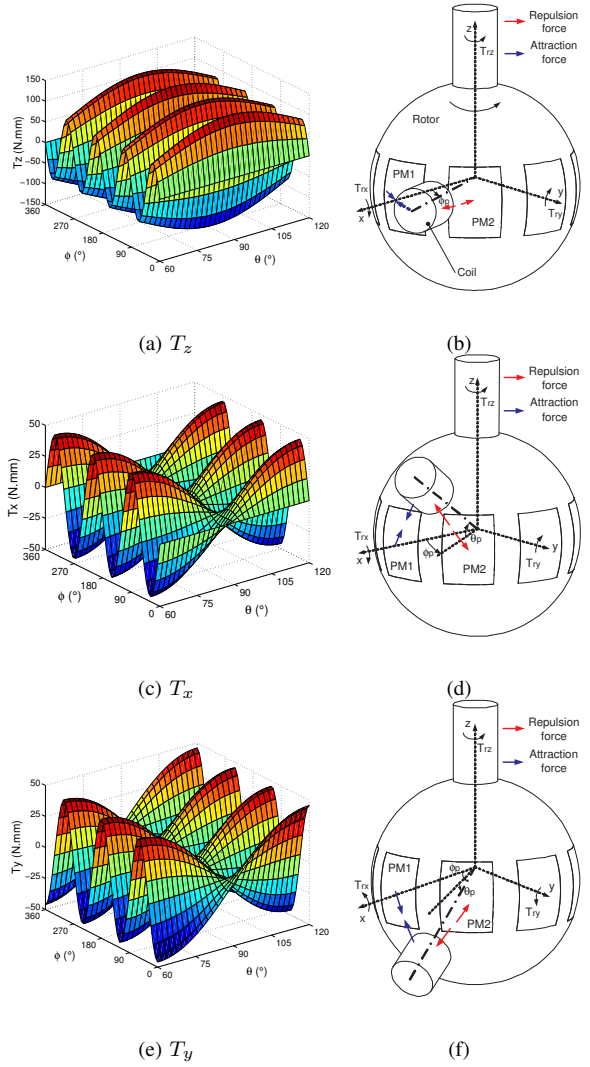

(a) T_z (b)

(c) T_x (d)

(e) T_y (f)

Fig. 7. Simulation of torque variation by a single coil

B. The Effect of Iron Stator on Torque Output

As the iron stator affects the magnetic field distribution of PM rotor [18], it may also change the actuator torque output. The following study is based on a fix-sized rotor ($R_r = 45$mm). Let radii of the coil be fixed ($R_0 = 45.1$mm, $R_1 = 50$mm) and stator size start increasing from 50mm. From Eqn. (20), it is know that $R_c = O_{4,6}R_{c,1} + O_{4,5}R_{c,2}$, where $O_{4,5}$ and $O_{4,6}$ can be calculated from stator radius R_s. The computed relationship between R_c and R_s is presented in Fig. 8(a). It can be observed that the actuator torque is larger with a smaller size of stator. Imagine an iron stator with infinite size, which is equivalent to a stator made from non-magnetic materials such as aluminium. Thus, when the stator is made from non-magnetic materials, R_c is equal to the lowest value in Fig. 8(a) (4.2×10^4mm^4). The iron stator with 50mm radius can increase the actuator torque by 60%.

The second study is based on a flexible coil, i.e., the external radius of coil R_1 is equal to the stator radius R_s.

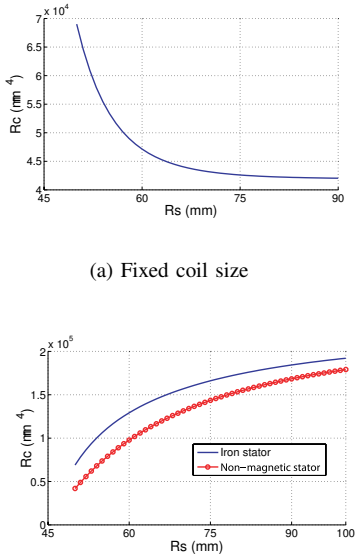

(a) Fixed coil size

(b) Variable coil size

Fig. 8. Relationship between torque output and stator radius (R_c vs. R_s)

Therefore, R_1 will follow the change of R_s. The relationship between R_1 and R_s is plotted in Fig. 8(b). To analyze the effect of iron stator, the relationship between R_1 and R_s with an aluminum stator is also calculated and presented with a dotted line. From Fig. 8(b), it can be seen that the iron stator does help to increase the actuator torque.

C. Ratio Selection of Rotor/Stator Radii

The previous study is based on a rotor with fixed size. However, in actuator design, people normally fix the stator size, and find the relationship between torque constant and the ratio of rotor/stator radii. From this relationship, an optimum ratio can be selected, and thus the rotor size can be obtained. This approach can offer some advantages such as:

- The optimization design of the actuator can be considered based on the performance of the whole system including stator and rotor, instead of individual components.
- The stator radius can be determined in the first place, to satisfy the requirements of maximum actuator size in different situations.
- The use of ratio between rotor and stator radii can be regarded as a nondimensional method, so that it is able to analyze the actuator performance without considering the specific dimensions.

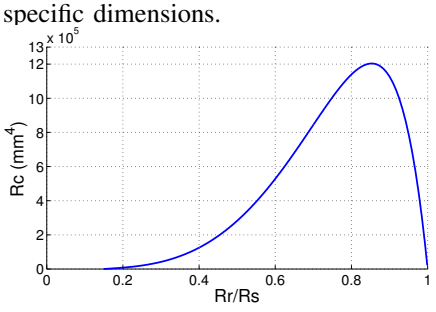

Fig. 9. Relationship between R_c vs. R_r/R_s

The relationship between R_c in torque constant and R_r/R_s is illustrated in Fig. 9. The maximum value of R_c happens at $R_r/R_s = 0.85$ approximately. This curve can be explained in a physical perspective. When R_r/R_s is very low, the rotor size is small, and thus the flux density generated by the rotor is low. As a result the value of R_c is very small. With the increase of R_r/R_s, R_c increases. However, when R_r/R_s is larger than a certain degree, the coil winding is smaller ($R_0 \geq R_r$ and $R_1 = R_s$). Therefore, R_c and torque output of the actuator decreases.

VI. Conclusion

This paper studied the torque output of a 3-DOF PM spherical actuator with a iron stator. The mathematic model of the torque output was derived. The effect of the iron stator on the actuator torque output was analyzed. It is found that the employment of laminated iron for the stator fabrication can increase the actuator torque up to 60%. In addition, relationship between torque constant and rotor & stator parameters was plotted according to the mathematic models, which can facilitate the optimization design of the spherical actuator.

Acknowledgment

This work is funded under collaborative research project grant U02-A-O40B for Nanyang Technological University, Singapore Institute of Manufacturing Technology, Singapore and Georgia Institute of Technology, USA. The authors acknowledge the assistance from Mr. Jialin Su, Dr. Weihai Chen and Mr. Thomas Thng.

References

[1] F. C. Williams, E. R. Laithwaite, and J. Eastham, "Development and design of spherical induction motors," *Proceedings of IEE*, pp. 471–847, Decemeber 1959.

[2] E. R. Laithwaite, "Design of spherical motors," *Electrical Times (London)*, vol. 9, pp. 921–925, June 1960.

[3] K. Davey, G. Vachtsevanos, and R. Powers, "The analysis of fields and torques in spherical induction motors," *IEEE Transactions on Magnetics*, vol. 23, no. 1, pp. 273–282, January 1987.

[4] G. J. Vachtevanos, K. Davey, and K. M. Lee, "Development of a novel intelligent robotic manipulator," *IEEE Control Systems Magazine*, vol. 7, no. 3, pp. 9–15, June 1987.

[5] K. M. Lee and C. K. Kwan, "Design concept development of a spherical stepper for robotic applications," *IEEE Transactions on Robotics and Automation*, vol. 7, no. 1, pp. 175–181, February 1991.

[6] K. M. Lee, R. B. Roth, and Z. Zhou, "Dynamic modeling and control of a ball-joint-like variable-reluctance spherical motor," *ASME Journal of Dynamic Systems, Measurement, and Control*, vol. 118, pp. 29–40, March 1996.

[7] J. Wang, G. W. Jewell, and D. Howe, "Analysis, design and control of a novel spherical permanent-magnet actuator," *IEE Proceedings: Electric Power Applications*, vol. 145, no. 1, pp. 61–71, January 1998.

[8] W. Wang, J. Wang, G. W. Jewell, and D. Howe, "Design and control of a novel spherical permanent magnet actuator with three degrees of freedom," *IEEE/ASME Transactions on Mechatronics*, vol. 8, no. 4, pp. 457–468, December 2003.

[9] J. Wang, G. W. Jewell, and D. Howe, "A novel spherical actuator: design and control," *IEEE Transactions on Magnetics*, vol. 33, no. 5, pp. 4209–4211, September 1997.

[10] ——, "A novel spherical permanent magnet actuator with three degrees-of-freedom," *IEEE Transactions on Magnetics*, vol. 34, no. 4, pp. 2078–2080, July 1998.

[11] G. S. Chirikjian and D. Stein, "Kinematic design and commutation of a spherical stepper motor," *IEEE/ASME Transactions on Mechatronics*, vol. 4, no. 4, pp. 342–353, December 1999.

[12] K. Kahlen, I. Voss, C. Priebe, and R. W. De Doncker, "Torque control of a spherical machine with variable pole pitch," *IEEE Transactions on Power Electronics*, vol. 19, no. 6, pp. 1628–1634, November 2004.

[13] K. M. Lee, H. Son, and J. Joni, "Concept development and design of a spherical wheel motor (SWM)," *Proceedings of the 2005 IEEE/ASME International Conference on Robotics and Automation*, pp. 335–340, July 2005.

[14] K. M. Lee and H. Son, "Torque model for design and control of a spherical wheel motor," *Proceedings of the 2005 IEEE/ASME International Conference on Advanced Intelligent Mechatronics*, pp. 335–340, July 2005.

[15] L. Yan, I. M. Chen, C. K. Lim, G. L. Yang, W. Lin, and K. M. Lee, "Experimental investigation on the magnetic field of a permanent magnet spherical actuator," *2005 IEEE/ASME International Conference on Advaned Intelligent Mechatronics*, pp. 341–346, July 2005.

[16] L. Yan, I. Chen, G. Yang, and K. Lee, "Analytical and experimental investigation on the magnetic field and torque of a permanent magnet spherical actuator," *IEEE/ASME Transactions on Mechatronics*, vol. 11, no. 4, pp. 409–419, August 2006.

[17] L. Yan, I. Chen, C. Lim, G. Yang, W. Lin, and K. Lee, "Design and analysis of a permanent magnet spherical actuator," *IEEE/ASME Transactions on Mechatronics*, vol. 13, no. 2, pp. 239–248, April 2008.

[18] ——, "Magnetic field analysis of spherical actuators with iron stator," in *2008 IEEE International Conference on Robotics, Automation and Mechatronics*, Chengdu, China, June 2008, pp. 1050–1055.